Organized Nature of a Turbulent Trailing Vortex

Promode R. Bandyopadhyay*
NASA Langley Research Center, Hampton, Virginia 23665
and
Daniel J. Stead† and Robert L. Ash‡
Old Dominion University, Norfolk, Virginia 23508

Experiments have been carried out into the turbulence structure of a low-Reynolds-number ($15 \times 10^3 < Re_\Gamma < 25 \times 10^3$, based on the maximum azimuthal velocity and core diameter) trailing vortex produced at the juncture of a flow aligned cylinder and a pair of oppositely loaded airfoils. Five different types of screens are placed ahead of the vortex generator. Components of the mean velocity, Reynolds stress flux, and quasiperiodic large-scale wavelengths have been measured. The turbulence structure varies with Rossby number. The vortex core is not a benign solid body of rotation. It has intermittent patches of turbulent and laminarescent fluid. The shear-stress-rich low-momentum core fluid intermittently ejects outwards in the direction of vortex rotation.

I. Introduction

IT is now well accepted that the dynamics of many turbulent shear flows is largely determined by quasiorganized motions.[1] The existence of a deterministic nature opens the possibility of flow control. So far, studies of organized motions have largely dealt with turbulent boundary layers, mixing layers, jets, and to lesser extent with wakes. However, it appears that there has been no similar study on trailing vortices (see Refs. 2 and 3, for example). It is not clear if there are organized motions involved in the production or dissipation of turbulence in a trailing vortex also. Identification of the organized motions in a low-Reynolds-number trailing vortex is the subject of this paper. This has been carried out in a trailing vortex subjected to a range of freestream turbulence.

II. Experiments

A. Wind Tunnel and Model

The experiments were carried out in the Low-Speed Boundary-Layer Channel of the NASA Langley Research Center. It is a closed-circuit wind tunnel. The nominal cross section is 61 × 91 cm and the test section length is 6.1 m. The tunnel roof and floor were adjusted to generate a nominally zero pressure gradient along the test section. The present experiments were carried out at a reference incoming freestream velocity of 15 m/s.

The model used to produce the trailing vortex is shown in Fig. 1. It is essentially a flow aligned cylinder of diameter $d = 2.5$ cm. A pair of oppositely loaded airfoils are placed in the longitudinal plane of the cylinder to generate a trailing vortex. The absolute value of the angle of attack is 8 deg in each airfoil. The airfoils have an NACA 0012 section and the chord c and span are 10.2 and 44.5 cm, respectively. Hoffman and Joubert[4] and Leuchter and Solignac[5] have used similar arrangements to produce trailing vortices in wind tunnels.

The freestream turbulence was produced by screens and grids located downstream of the contraction and 30.5 cm upstream of the model. Figure 2 shows the screens and grids schematically, and their dimensions as well as the freestream turbulence levels at the leading- and trailing-edge locations of the airfoils are given in Table 1. The detailed spectra and the streamwise variation of the turbulence intensity are given in Ash and Stead.[6]

B. Measurements

The measurements and flow visualization were carried out at an axial distance $x = 40c$. An HP100 series A600 computer was used to control the traverse and the data-acquisition system. The traverse was capable of determining the location within 0.025 mm. Typically, each radial traverse of 40 mm had about 30 data points.

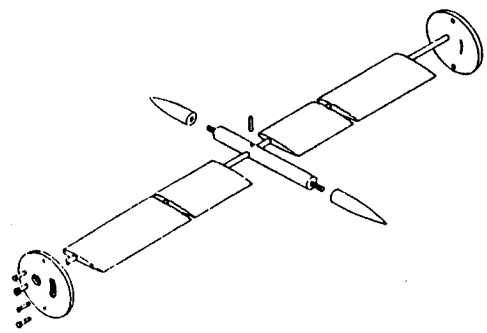

Fig. 1 Model assembly showing flow aligned cylinder and airfoils.

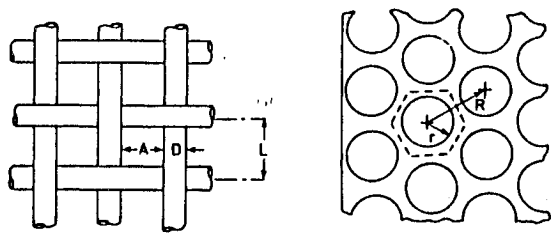

Fig. 2 Screens and grids used to generate freestream turbulence (see Table 1).

Presented as Paper 90-1625 at the AIAA 21st Fluid Dynamics, Plasma Dynamics, and Lasers Conference, Seattle, WA, June 18–20, 1990; received Aug. 22, 1990; revision received Dec. 3, 1990; accepted for publication Dec. 3, 1990.

*Senior Research Associate, Mail Stop 170. Also Adjunct Professor, Mechanical Engineering and Mechanics Department, Old Dominion University. Associate Fellow AIAA.

†Graduate Student.

‡Professor and Chairman, Mechanical Engineering and Mechanics Department. Associate Fellow AIAA.

Table 1 Geometrical properties of turbulence generators (see Fig. 2 for symbols)

Freestream/geometry	Holes/cm	D or R, mm	A or r, mm	Material	Percent open	$\frac{u'}{U_\infty}\Big\|_{\text{t.c.}}$	$\frac{u'}{U_\infty}\Big\|_{\text{t.c.}}$
Unmodified	—	—	—	—	100	0.00032	0.00034
Fine screen	7.9	0.41	0.86	Steel	46.2	0.0113	0.0074
Small grid	2.1	4.76	3.97	Aluminum	63.0	0.0148	0.0111
Coarse screen	3.9	0.81	1.72	Steel	46.2	0.0126	0.0101
Large grid	0.57	17.5	12.7	Steel	48.0	0.0485	0.0389

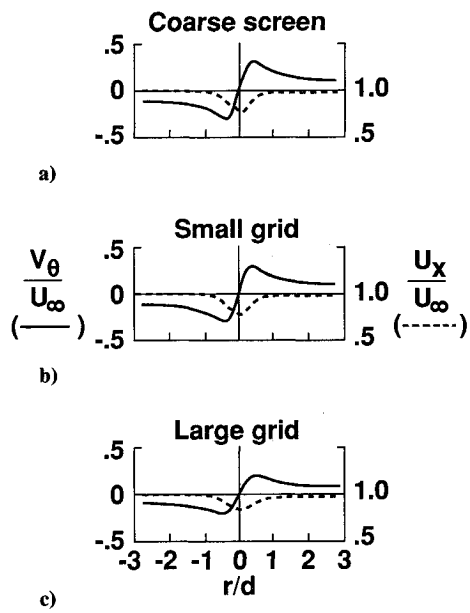

Fig. 3 Azimuthal and axial mean velocity distributions at x/c = 40 in a) coarse-screen, b) small, and c) large-grid cases. Seven-hole probe data.

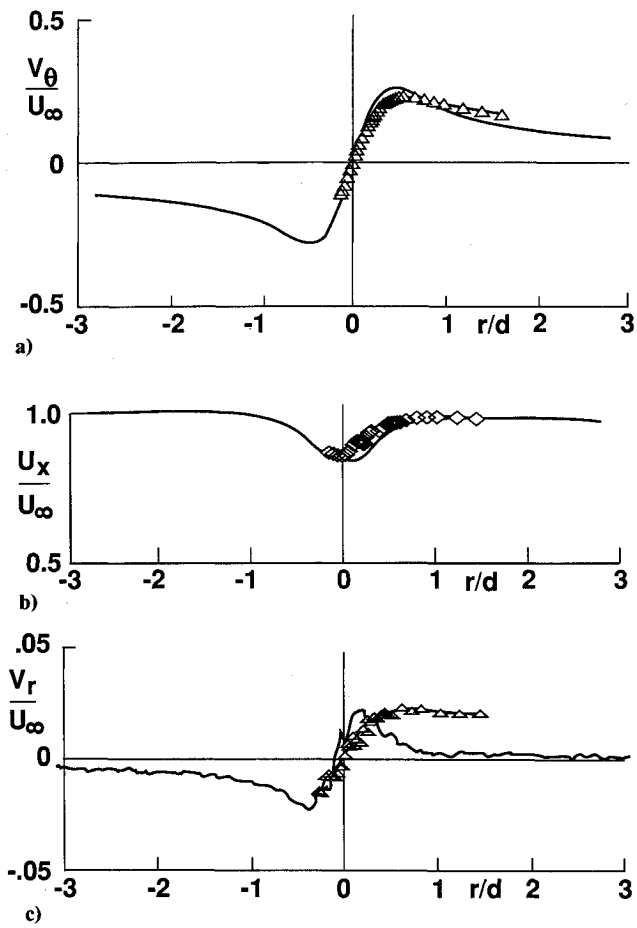

Fig. 4 Fine-screen case: a) azimuthal, b) axial, and c) radial velocity distributions at x/c = 40. Solid line: Seven-hole probe data; symbols: x-wire data.

1. Seven-Hole Pitot Measurements

The three-dimensional mean velocity field has been surveyed extensively using a seven-hole probe for the five freestream turbulence cases investigated. The probe had a conical tip with a half-angle of 30 deg. The outside diameter of the probe was about 2.5 mm. As far as blockage is concerned, this compares with 3 mm in the single hot-wire probe. It is estimated that the probe is capable of resolving velocity magnitude and direction at incident flow angles up to 75 deg with respect to the probe axis.[7]

2. Hot-Wire Measurements

The turbulence measurements have been carried out with DISA miniature x-wire and single-wire probes. The wires were run by TSI constant-temperature anemometers. The signal was digitized using an Analogic DATA6100 signal processor. A total of 25 records of 32,758 readings per record at a sampling rate of 50 μs between readings were used in the averaging of the hot-wire data. The spectra were collected with an HP Spectrum Analyzer using 256 traces each containing 512 data points sampled at 500-μs intervals and giving a total record length of 65.536 s and a bin size of 4 Hz. The turbulence data were collected in a vertical traverse through the vortex center, which was determined as the point of minimum mean velocity and the spanwise point of symmetry in the turbulence intensity profiles.

3. Flow Visualization

Smoke flow visualization of the trailing vortex was carried out in general illumination using a xenon lamp light source. The smoke was injected through a hollow afterbody from an external smoke generator. The smoke was piped through one of the airfoil pivot tubes (Fig. 1). Videotape records were made of the flow visualization. The pictures were digitized subsequently and processed using the facilities of the Image Processing Laboratory of NASA Langley Research Center. To determine the three wavelengths reported here, the digitized pictures were projected on a large screen and the wavelengths were read using a track ball and the displayed pixel locations. The beginning and the end of a wave were, however, judged manually.

III. Results and Discussion

A cylindrical coordinate system, viz., (x, r, θ), where the mean and fluctuating velocities are, respectively, U_x, u_x; V_r, u_r; and V_θ, u_θ, is used. These velocities are positive in the downstream, radially outwards and in the direction of the vortex rotation, respectively. The origins of x and r are at the trailing edge of the airfoil and the vortex center, respectively.

A. Mean Velocity Characteristics

The far downstream (x/c = 40) azimuthal V_θ and axial velocity U_x profiles obtained with the seven-hole probe for the coarse screen, small and large grid freestream cases, are shown in Fig. 3. In Figs. 4 and 5, in the fine-screen and

unmodified cases, the seven-hole probe and x-wire measurements of V_θ, U_x, and V_r are compared. The U_x distributions are wakelike in all freestream turbulence cases. However, note that the wakes do not spread with downstream distance [$d_c \approx \mathcal{O}(d)$ even at $x = 40c$] indicating the presence of a controlling mechanism. The radial distributions of V_θ and V_r have similar trend. In order of magnitude terms, $(U_\infty - U_{cl}) = \mathcal{O}(V_{\theta\max}) = \mathcal{O}(10V_{r\max})$, where cl and max stand for centerline and maximum values, respectively. The vortex core Reynolds number Re_Γ is defined as Γ/ν, where Γ is circulation, given by $\pi d_c V_{\theta\max}$ and ν is kinematic viscosity of the fluid; here, d_c is core diameter and $V_{\theta\max}$ is the maximum azimuthal or swirl velocity V_θ that is reached at $r = d_c/2$. From the seven-hole probe mean velocity profile measurements, it is estimated that the value of Re_Γ and the mean kinetic energy in the core is the highest in the fine-screen case[6] (Table 1). The seven-hole probe measurements of the mean velocity components are estimated to be more accurate than those from the x-wire.

B. Turbulence Structure

1. Reynolds Stresses and Their Flux

The fine-screen double and triple moments are shown in Figs. 6 and 7, respectively. The two respective moments in the unmodified case are shown in Figs. 8 and 9. The fine-screen turbulence distributions are radially spread out over, approximately, $r = d$ but they extend over only $r = 0.5d$ in the unmodified case. However, the distributions of the mean velocity V_θ extends over a large r. In order-of-magnitude terms, compared to those in the unmodified case, the absolute values of the double and triple moments are about 20 and 100 times larger, respectively, in the fine-screen case.

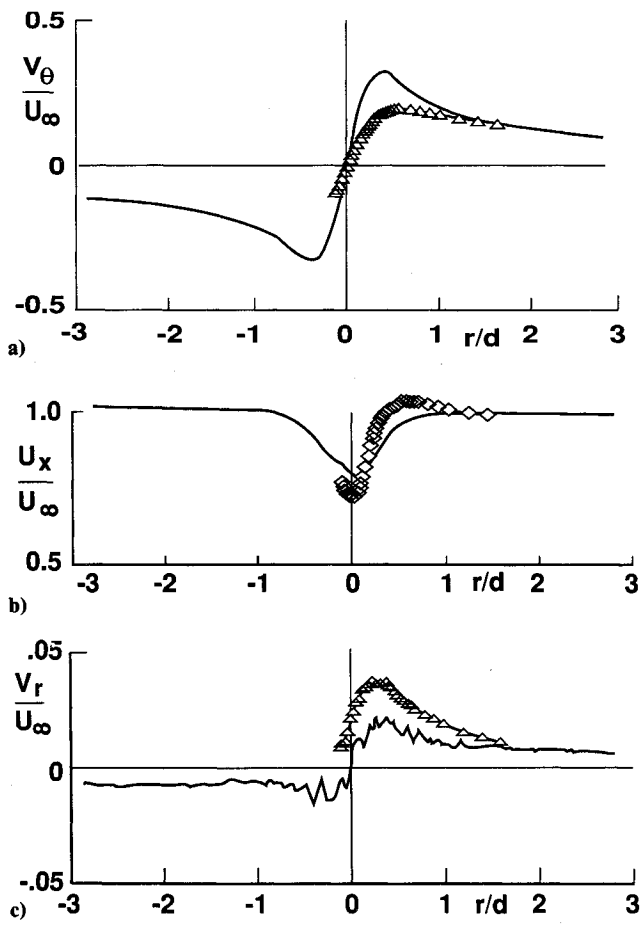

Fig. 5 Unmodified case: a) azimuthal, b) axial, and c) radial velocity distributions at $x/c = 40$. Solid line: Seven-hole probe data; symbols: x-wire data.

The diffusion measurements in Figs. 7 and 9 retain the signs. They are also long-time averaged measurements and no threshold setting is involved as is common in coherent structure studies. Therefore, statistical interpretations of the nature of the organized motions in the vortex can be made with confidence. The following discussion about flux is concerned with the vortex excepting a small region in the core ($0 \le r/d \le 0.1$). In the fine-screen case, statistically, $\overline{u_x^3}$ is negative but, $\overline{u_\theta^3}$ and $\overline{u_r^3}$ are both positive (overbars indicate long-time averages). Therefore, the direct stresses, viz., u_x^2 is transported longitudinally by the decelerating motions, while u_θ^2 and u_r^2 are transported in the direction of the vortex rotation and radially outward, respectively. Similarly, note that statistically, $(\overline{u_x^2 u_r})$ and $(\overline{u_x^2 u_\theta})$ are positive but $(\overline{u_x u_r^2})$ and $(\overline{u_x u_\theta^2})$ are negative. The shear stresses are negative. Therefore, it is concluded that the shear stresses $(-u_x u_r)$ and $(-u_x u_\theta)$, statistically, are transported radially outwards and in the direction of the vortex rotation by motions that are decelerating in the flow direction. The statistics also imply that the shear-stress causing motions come primarily from the second (Q2: $-u_x$, $+u_\theta$; $-u_x$, $+u_r$) rather than the fourth (Q4: $+u_x$, $-u_\theta$; $+u_x$, $-u_r$) quadrant. Since in a turbulent flow shear stress is contained in small-scale three-dimensional spiralling vorticity layers, the above results mean that intermittently, small three-dimensional packets of vorticity are being ejected outwards in the direction of rotation.

Measurements (given in the conference version of this paper) have shown that the turbulence characteristics in the

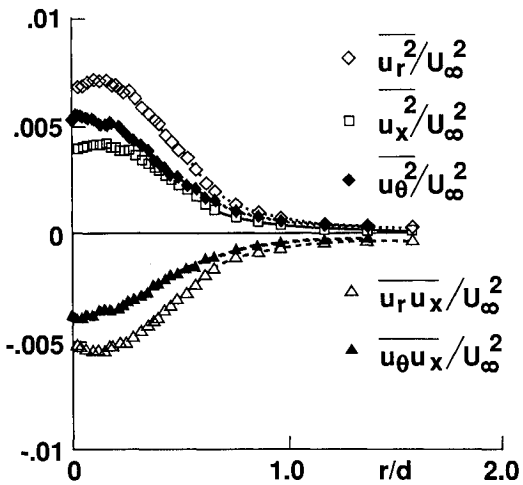

Fig. 6 Double moments at $x/c = 40$ in the fine-screen freestream case.

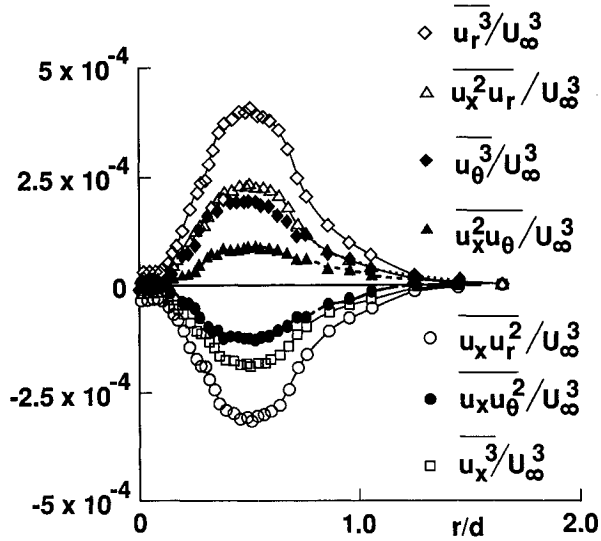

Fig. 7 Triple moments at $x/c = 40$ in the fine-screen freestream case.

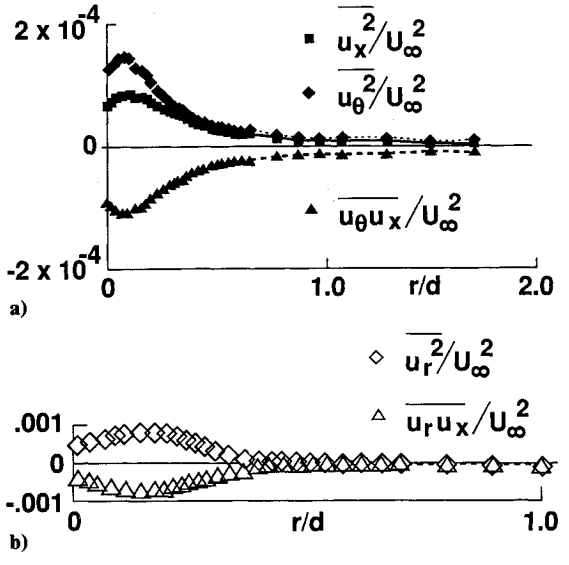

Fig. 8 Double moments at $x/c = 40$ in the unmodified freestream case.

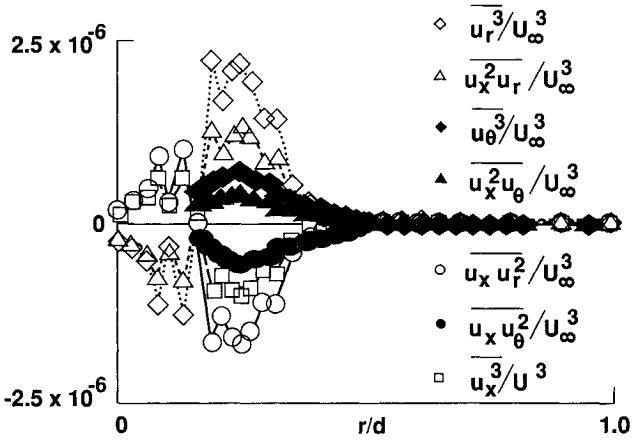

Fig. 9 Triple moments at $x/c = 40$ in the unmodified freestream case.

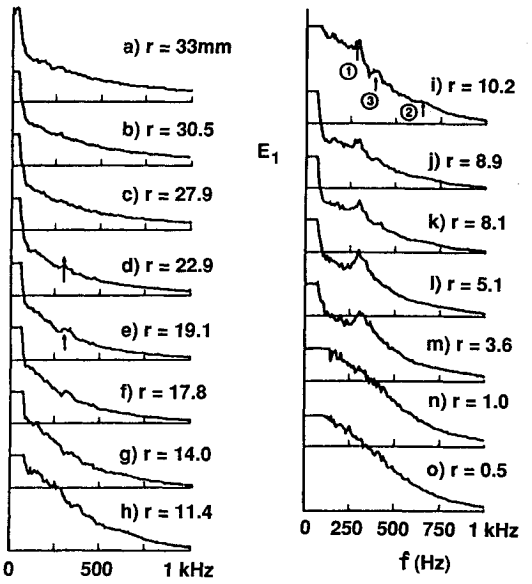

Fig. 10 Power spectra across the vortex at $x/c = 40$ in the fine-screen freestream turbulence case.

small-grid case are also weak and virtually identical to those in the unmodified case. So, it is interesting that they are considerably stronger in the fine-screen case. Batchelor[8] has shown that, in a (laminar) line vortex, as the azimuthal velocity decays, an axial pressure gradient develops which also gives rise to an axial component of the velocity. In the present experiments, the seven-hole probe measurements show that the centerline axial velocity defect ($U_\infty - U_{cl}$) is the lowest, viz., 2.68 m/s in the fine-screen case. It is about the same in the remaining two cases, viz., 3.82 m/s in the unmodified case and 3.56 m/s in the small-grid case. The value of $d_c = 24.0$ mm in the fine-screen case but it is nearly equal in the unmodified (= 19.2 mm) and the small-grid (= 18.7 mm) cases. Also, $V_{\theta max}$ is the lowest (= 4.1 m/s) in the fine-screen case, but it is higher in the unmodified (= 5.0 m/s) and the small-grid (= 4.7 m/s) cases. Morton[9] has argued that the pressure gradient is important when Long's[10] parameter $F/\Gamma_o^2 = \mathcal{O}(1)$, where F is a force variable and Γ_o is circulation in the initial roll-up region. Measurements show that the mean and turbulence characteristics of a trailing vortex are strongly dependent on the magnitude of the Long's parameter. Since in the fine-screen cases, d_c is higher and $V_{\theta max}$ is lower, it is suspected that, in this case, V_θ has the maximum diminution, and therefore $abs(F/\Gamma_o^2)$ is also the highest of the three cases.[11] Since the model lift and drag would be the same *if* the effect of freestream turbulence is ignored, it is suggested that compared to the unmodified and the small-grid cases, the fine screen is capable of altering the initial vortex roll-up process that affects the downstream redistribution of the velocity and pressure components.

2. *Power Spectra*

The power spectra of the axial velocity fluctuation across the vortex in the fine-screen case are shown in Fig. 10. Three observations can be made. First, three dominant frequencies appear at $r = 10.2$ mm, that is approximately where the turbulence flux reaches a maximum or a minimum. The peaks are marked in Fig. 10(i). Frequencies 1 and 2 are at about 275 Hz and 650 Hz, respectively. It is believed that frequency 2 is like a rooster tail, that is, one having several closely spaced frequencies. (Rooster tails are known to be the result of the locking of two frequencies.) The jitter in the driving frequencies is probably the cause of the broadness of the hump in frequency 2. Work is continuing to determine if the frequencies 1 and 2 pertain to the axisymmetric and helical modes observed by Singh and Uberoi.[12] Frequency 3 is at 385 Hz and its presence does not seem to have been reported before. Second, Fig. 10(l) shows the appearance of a dominant frequency of about 300 Hz at $r = 5.1$ mm. This location is where the turbulence intensity reaches its maximum value (Fig. 6). Third, in the inner region, viz., $r < 5.1$ mm, where the diffusion terms are weak, there is no very obvious dominant frequency but the spectra are not at all smooth. The observations suggest that the turbulence diffusion might be related to the appearance of several dominant frequencies.

3. *Effect of Reynolds and Rossby Numbers and Freestream Turbulence Intensity*

It was pointed out earlier that the turbulence intensity and flux characteristics are very different in the fine-screen case and is virtually the same in the unmodified and the small-grid cases. A possible explanation will be discussed here. Table 1 shows that the freestream turbulence intensity level T_u is about the same in the fine-screen and the small-grid cases. It is much lower in the unmodified case. So the different characteristic of the turbulence in the fine-screen case is not ascribable to the intensity of the freestream turbulence.

Results presented later show that the turbulence is undergoing a partial relaminarization process intermittently. In a rotating fluid, this process can be expected to be determined by Rossby and Reynolds numbers.[13] In the present case, the Rossby number (Ro) has been simply defined as $(U_\infty - U_{cl})/U_{\theta max}$, where the numerator represents the inertial component

or the axial velocity defect and the denominator represents the Coriolis component. The vortex Reynolds number and Rossby number in the five freestream cases considered here have been calculated from the seven-hole probe mean velocity measurements and their variation is shown in Fig. 11. An interesting comparison can be made between the three cases out of the five where the turbulence measurements have been made. The value of Re_Γ is almost the same in the unmodified and the fine-screen cases but the fine screen has a significantly lower value of Ro. On the other hand, the unmodified and the small-grid cases have almost the same Ro and the unmodified case has a slightly higher Re_Γ. This clearly means that the Coriolis component is the highest in the fine-screen case. A lower Ro is expected to promote relaminarization. The results indicate that the turbulence structure in the three cases has been affected by Rossby number and not Reynolds number.

Some further insight can be obtained from a similar plot of the relaminarization process in a rotating channel. The laminar, turbulent, and relaminarizing zones have been documented by Johnston et al.[14] In that flow, Narasimha and Sreenivasan[13] have pointed out that there is no unique value of Re or Ro for relaminarization. At any given Reynolds number, there is a range of Rossby numbers where relaminarization can take place. The trailing vortex probably also has a similar behavior. A larger variation in the Reynolds number than achieved here is apparently needed to affect a change in the turbulence structure.

C. Relaminarization and the Dominant Wavelengths

Three views of the smoke-filled vortex are shown in Fig. 12. The first (Fig. 12a) is characterized by a low-smoke-density conical core region that is also wavy. The second (Fig. 12b) is characterized by periodically appearing bellows at the outer edges. The third (Fig. 12c) is a contoured version of Fig. 12b. The contour-free regions denote a relatively lower smoke density. The contours in Fig. 12c have been interpreted to mean that they represent two helical vortices winding around

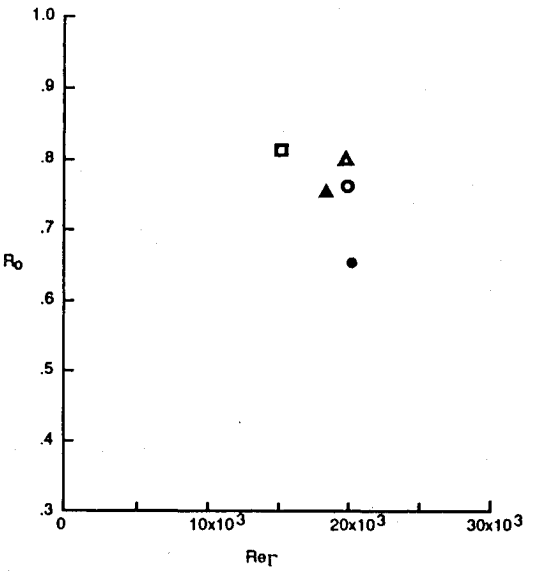

Fig. 11 Reynolds-number vs Rossby-number plot in the five freestream turbulence cases; ○: unmodified freestream; ●: fine screen; ▲: small grid; △: coarse screen; and □: large grid.

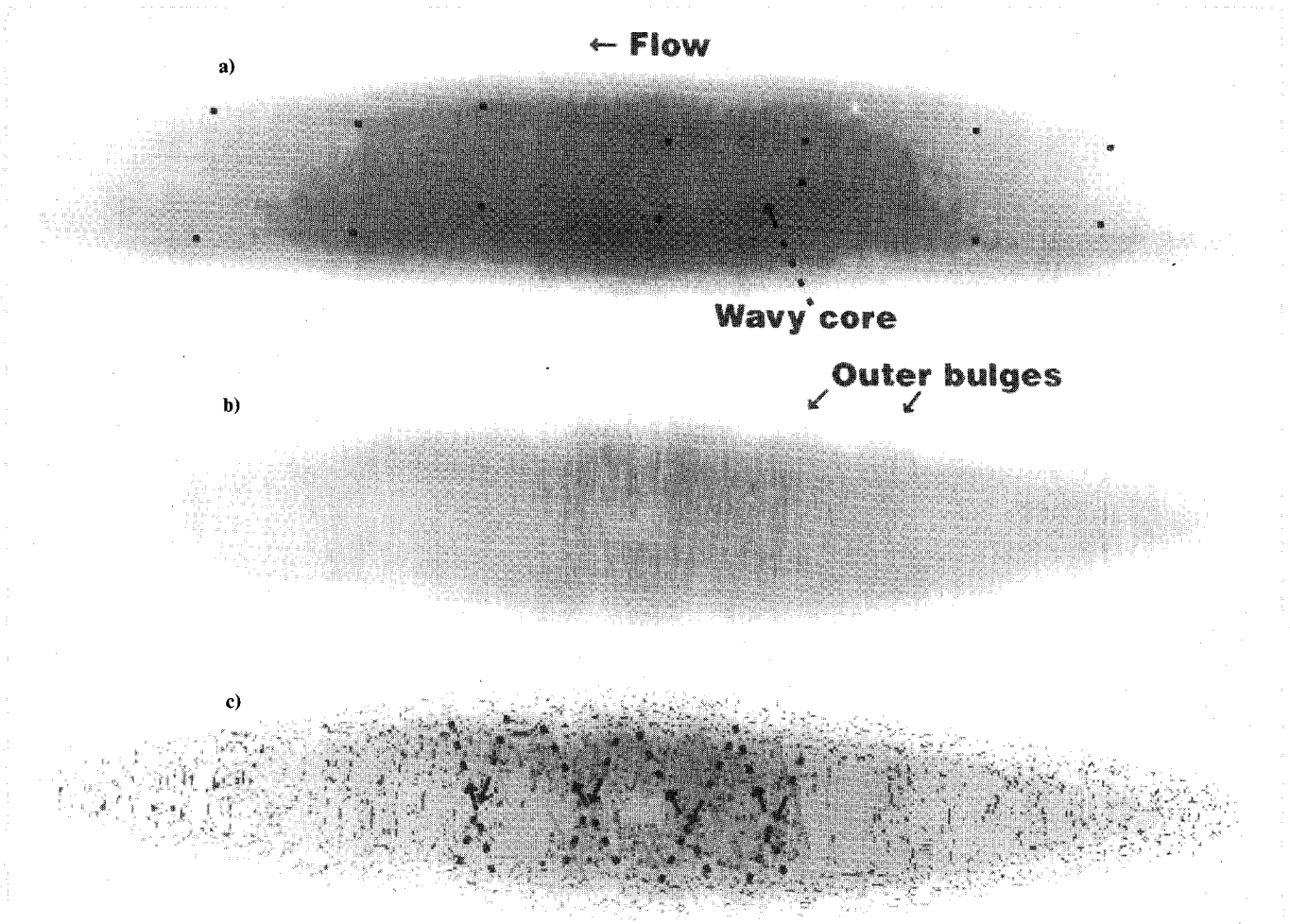

Fig. 12 Longitudinal views of the smoke-filled vortex at $x/c = 40$ in the fine-screen case. Flow is from right to left. Contours represent smoke density: a) shows relaminarizing conical wavy cores; b) shows bellows at the outer edge; and c) suggests a helical vortex pair crossing.

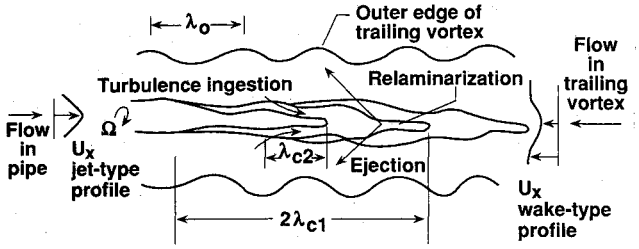

Fig. 13 Schematic representation of the turbulence structure of the vortex.

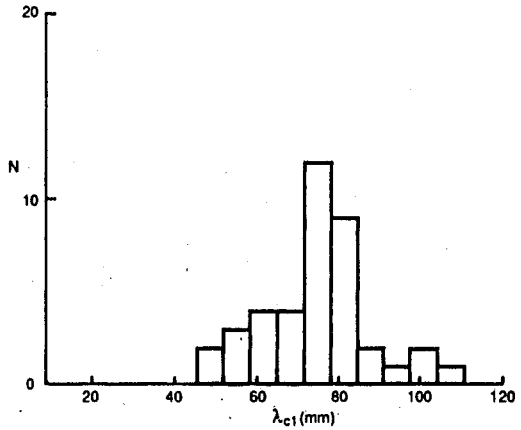

Fig. 14 Histogram of the core wavelength λ_{c1}. Bars are 6.6 mm wide and centered at 74.7 mm.

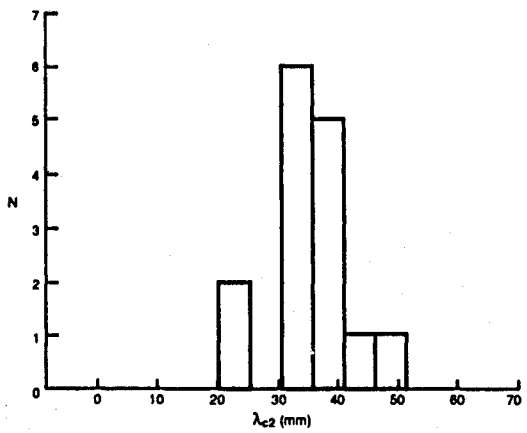

Fig. 15 Histogram of the core wavelength λ_{c2}. Bars are 5.2 mm wide and centered at 33.1 mm.

the outer edge of the trailing vortex in opposite corkscrew fashions. It is suggested that these two helical vortices originate from the two junctions between the two oppositely loaded airfoils and the flow aligned cylinder. Conceivably, this aspect is absent in a trailing vortex originating from a wing tip.

It is reasonable to suspect that the wavy conical core in Fig. 12a represents a relaminarizing region. Thus, it is instructive to compare this flow with the low-Reynolds-number relaminarization process as it occurs in the so-called puff in a pipe. It is encouraging to see that the relaminarized region in a puff is also conical (Fig. 7 in Ref. 15). It may be of significance that both the puff and the trailing vortex contain helical motions. There are two wavelengths, viz., λ_{c1} and λ_{c2}, associated with the visualized core of the trailing vortex and they are defined in Fig. 13. The third significant wavelength λ_o, associated with the outer edge as shown in Fig. 12b is also defined in Fig. 13. The histograms of the measured values of the three wavelengths are shown in Figs. 14–16. The two core wave-

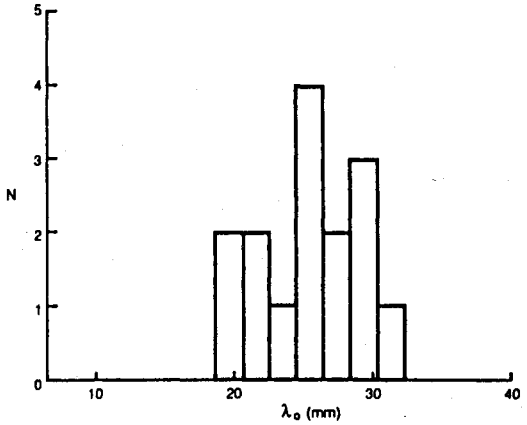

Fig. 16 Histogram of the outer-edge wavelength λ_o. Bars are 1.96 mm wide and centered at 25.4 mm.

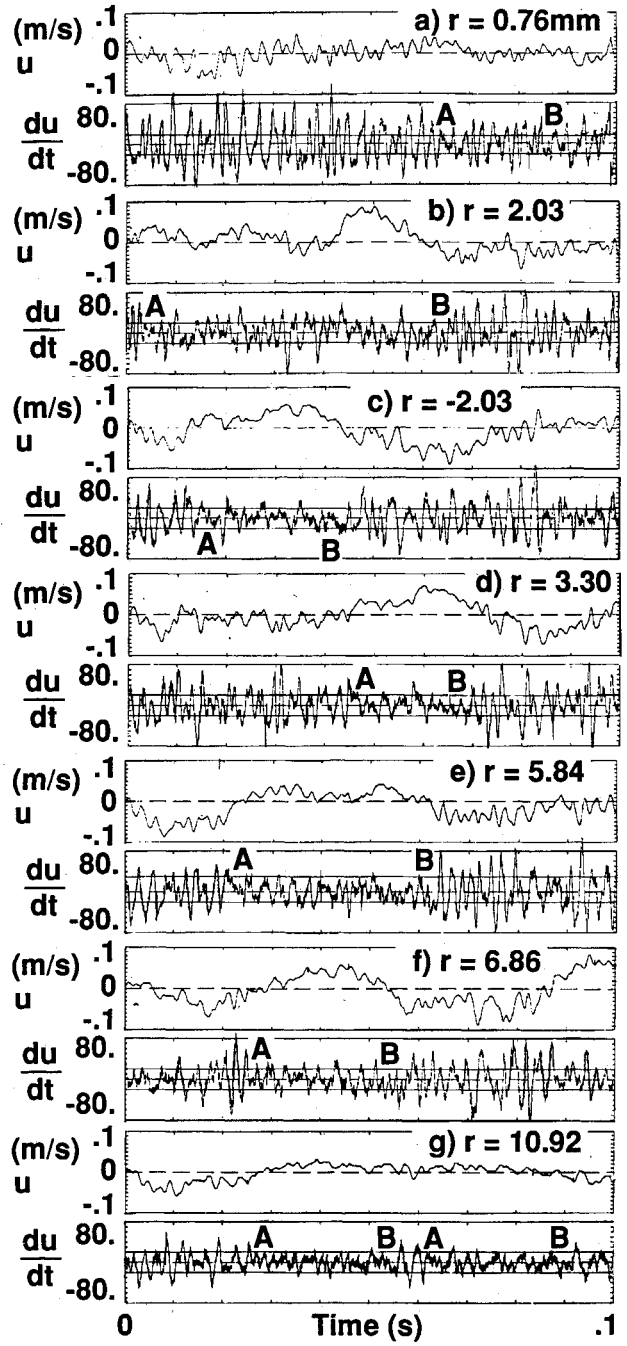

Fig. 17 Signatures of fluctuating velocity and its time derivative across the vortex at $x/c = 40$ in the fine-screen freestream turbulence case. Time periods marked "AB" represent a relatively "quieter" period.

Table 2 Summary of the dominant wavelengths

λ_{c1}/d_c	λ_{c2}/d_c	λ_o/d_c
3.1	1.4	1.06

lengths, viz., λ_{c1} and λ_{c2}, seem to have a slightly smaller standard of deviation than λ_o does. Table 2 contains the mean values nondimensionalized by the core diameter obtained from the seven-hole probe measurements of the mean azimuthal velocity distribution.

Table 2 shows that the wavelengths scale with the core diameter d_c. It is interesting to note that λ_{c1}/d_c is nearly equal to π (and $2\lambda_{c2} \simeq \lambda_{c1}$). Dinkelacker[16] has pointed out that in a reattaching backward-facing step flow that is dominated by overturning motions (Ref. 17), the ratio of the periodic spacing of the large structures to the step height also has the same value.

An independent support of the relaminarization process is obtained from hot-wire measurements. How the resultant velocity fluctuation (u) trace varies across the vortex is shown in Fig. 17. Below each velocity trace, its time derivative trace, viz., du/dt, is also shown. The du/dt signal shows more clearly that if a threshold of ± 20 units is chosen all across the vortex, the motion is characterized by long quiescent periods (marked AB in Fig. 17) followed by periods of high turbulence activity. This feature of the du/dt trace compares well with that in the turbulent puff in a pipe (Fig. 3 in Ref. 18). The significance of the u and the du/dt signals is that they can be used to measure (du^2/dt) which is a gross measure of the rate of change of the turbulent kinetic energy. A statistical analysis of the relaminarization information in Fig. 17 is currently underway.

The structure of the trailing vortex at the downstream station, viz., $x/c = 40$, is described schematically in Fig. 13. The turbulence measurements have shown that the vortex core is not a benign solid body of rotation but has a dynamic nature. There is an intermittent exchange of momentum between the outer and the core regions. The core receives a patch of turbulent fluid and the rotational motion partially relaminarizes it. This process in the trailing vortex is in some ways the mirror image analogue of that in a puff in a low-Reynolds-number pipe flow. This aspect is emphasized in Fig. 13.

IV. Conclusions

A trailing vortex experiment has been carried out in the following ranges: $0.032\% \leq T_u \leq 1.48\%$, $15 \times 10^3 \leq Re_\Gamma \leq 25 \times 10^3$, and $0.65 \leq Ro \leq 0.81$. Within this parameter range, the screens, but not the freestream turbulence level, are able to produce significant variations in the turbulence structure of the vortex. It remains to be ascertained if the ratio of the scale of freestream turbulence to the shear layer thickness is critical to the initial roll-up process. Also, Ro had a stronger effect on the turbulence structure than that due to Re_Γ.

The turbulence structure in the trailing vortex having the lowest Ro has been studied in detail. The conventional view, viz., that the vortex core is a benign solid body of rotation, is untenable at least in this case. The core has a wavelike character. There are intermittent patches of highly turbulent and partially relaminarized fluid in the core. The exchange of momentum between the outer turbulent region and the core is carried out by organized motions. The shear-stress-rich low-momentum core fluid intermittently ejects outward in the direction of vortex rotation.

Acknowledgments

The support of NASA is acknowledged (P. R. Bandyopadhyay: NAS1-18599; D. J. Stead and R. L. Ash: NAG1-530).

References

[1]Fiedler, H., "Coherent Structures in Turbulent Flows," *Progress in Aerospace Sciences*, Vol. 25, 1988, pp. 231–269.

[2]Hall, M. G., "The Structure of Concentrated Vortex Cores," *Progress in Aerospace Sciences*, Vol. 7, 1966, pp. 53–110.

[3]Leibovich, S., "Vortex Stability and Breakdown Survey and Extension," *AIAA Journal*, Vol. 22, No. 9, 1984, pp. 1192–1205.

[4]Hoffman, E. R., and Joubert, P. N., "Turbulent Line Vortices," *Journal of Fluid Mechanics*, Vol. 16, 1963, p. 395.

[5]Leuchter, O., and Solignac, J. L., "Experimental Investigation of the Turbulent Structure of Vortex Wakes," *Proceedings of the 4th Symposium on Turbulent Shear Flows*, Karlsruhe, Germany, 1983, p. 531.

[6]Ash, R. L., and Stead, D. J., "Influence of Freestream Turbulence on a Trailing Line Vortex," *Proceedings of the 3rd International Conference on Fluid Mechanics*, Vol. 1, Cairo, 1990, pp. 345–358.

[7]McGinley, C. B., "Three-Dimensional Mean Flow Experimental Study of Vortex Unwinding," M.S. Thesis, George Washington Univ., Washington, 1988.

[8]Batchelor, G. K., "Axial Flow in Trailing Line Vortices," *Journal of Fluid Mechanics*, Vol. 20, 1964, pp. 645–658.

[9]Morton, B. R., "The Strength of Vortex and Swirling Core Flows," *Journal of Fluid Mechanics*, Vol. 38, 1969, pp. 315–333.

[10]Long, R. R., "A Vortex in an Infinite Viscous Fluid," *Journal of Fluid Mechanics*, Vol. 11, 1961, pp. 611–626.

[11]Phillips, W. R. C., and Graham, J. A. H., "Reynolds-Stress Measurements in a Turbulent Trailing Vortex," *Journal of Fluid Mechanics*, Vol. 147, 1984, p. 353.

[12]Singh, P. I., and Uberoi, M. S., "Experiments on Vortex Stability," *Physics of Fluids*, Vol. 19, No. 12, 1976, pp. 1858–1863.

[13]Narasimha, R., and Sreenivasan, K. R., "Relaminarization of Fluid Flows," *Advances in Applied Mechanics*, Vol. 19, 1979, pp. 221–309.

[14]Johnston, J. P., Halleen, R. M., and Lezius, D. K., "Effects of Spanwise Rotation on the Structure of Two-Dimensional Fully Developed Turbulent Channel Flow," *Journal of Fluid Mechanics*, Vol. 56, Pt. 3, 1972, pp. 533–557.

[15]Bandyopadhyay, P. R., "Aspects of the Equilibrium Puff in Transitional Pipe Flow," *Journal of Fluid Mechanics*, Vol. 163, 1986, pp. 439–458.

[16]Dinkelacker, A., private communication, 1989.

[17]Jovic, S., and Browne, L. W. B., "Evolution of Coherent Structures in the Reattachment Region of a Separated Flow," *Proceedings of the 10th Australasian Fluid Mechanics Conference*, edited by A. E. Perry, Vol. I, University of Melbourne, Australia, 1989, pp. 8.31–8.34.

[18]Wygnanski, I., Sokolov, M., and Friedman, D., "On Transition in a Pipe Part 2, The Equilibrium Puff," *Journal of Fluid Mechanics*, Vol. 69, Pt. 2, 1975, pp. 283–304.